INTERNATIONAL JOURNAL OF
COASTAL, OFFSHORE & ENVIRONMENTAL ENGINEERING IJCOE Vol.8/No. 2/Spring 2023 (56-64)

*Available online at: www. Ijcoe.org*

# Investigation on the seasonal transformation of Tiab estuary's shoreline using RS and GIS techniques

**Maryam Rahbani [1,2], Danial Ghaderi [1,2*], Rahimeh Shamsaie [1], Zarafshan Salari [1], Ali Permas [3]**

[1] *Faculty of Marine Science and Technology, University of Hormozgan, Bandar Abbas, Iran*
[2] *Center Providing Consultation and Simulation Services for Coastal And Marine Environments, Bandar Abbas, Iran*
[3] *Hormozgan Province Ports & Maritime Authority, Shahid Rajaee Port Complex, Bandar Abbas, Iran*
*Corresponding Author: danialghaderi1@gmail.com*

**ARTICLE INFO**

*Article History:*
Received: 04 May. 2023
Accepted: 28 May. 2023

*Keywords:*
**Tiab Estuary**
**Strait of Hormuz**
**Shoreline Transformation**
**Sentinel-2**
**DSAS**

**ABSTRACT**

Estuaries are transition zones between the sea and land, and are constantly affected by tides. These areas are biologically important and sensitive. Tiab estuary, 7 km from away from the coast of Strait of Hormuz, is covered with mangroves and is also used for navigation by small commercial boats. This estuary is facing sedimentation issues nowadays which troubled navigation of vessels. Since the local wind conditions of the area is different seasonally, the influence of this difference on the transformation of the shoreline is considered for the years 2019 and 2020. The wind direction in the area is mainly SSW during summer, while is totally diverse during winter. Sentinel-2 satellite images have been used with similar water-level conditions. Normalized Difference Water Index and K-means algorithm are used for shoreline detection. The results show that the area of the estuary is more than 10 hectares smaller in summertime than in wintertime. The correlation coefficient of the seasonal transformation of the shoreline in 2019 and 2020 is 0.84, which shows that the seasonal transformation was similar in the two years. Shoreline transformation was at most along the curvatures of the river, whether in upstream or downstream. It was however varied between 45 and 200 m. Some dissimilarity in shoreline transformation was detected between the two years of study, specifically in upstream of the river, which is suggested to be due to human activities. It is believed that those parts of the estuary with high transformation are subject to permanent transformation in long term.

## 1. Introduction

Estuaries are the transitional zones between the sea and the rivers, which are mostly protected from wave affects, but still are constantly affected by the tide. These areas are biologically important and sensitive. Besides, anthropogenic factors can cause a wide range of changes in them (French, 2002). Various factors can change the processes of erosion and accretion in estuaries among them turbulence, variation of tidal cycles, the inflow of catchment area, local and swell waves, and climate change, (Schoellhamer, 2002). Erosion and accretion are constantly in progress in these areas own to the active hydrodynamic processes. Thus, minimal human (or natural) intervention, creates significant change in estuary zone (Ghaderi and Rahbani, 2021). Tiab estuary, located in Minab city, south of Iran, is one of the few navigable estuaries in this country. Tiab estuary faces sedimentation issue recently, in a way that emergency running aground of small fishing boats reportedly occurred. In this study, an attempt has been made to evaluate the short-term transformation of Tiab estuary's shoreline using RS and GIS techniques. To achieve this goal, the transform of the river shoreline in this estuary has been investigated during two consecutive years. The investigation is carried out for hot (summer) and cold (winter) seasons, to identify possible seasonal affect in shoreline transformation. Ghaderi and Rahbani, (2021), using field measurement, ANN and RS, investigated the amount of suspended sediments along the Tiab estuary. They claimed that the highest amount of suspended sediment can be found in the meanders of the estuary. Ghaderi and Rahbani, (2020a), using Landsat and Sentinel-2 satellite images, examined the

shoreline of Bandar Abbas city. They used Normalized Difference Water Index (NDWI) band ratio to identify water and land features, and Digital Shoreline Analysis System (DSAS) tool to calculate the amount of changes. They claimed the average shoreline change rate of the Bandar Abbas urban area is +2.35 m/year, and about 53% of the shoreline faces low accretion (0.5 to 10.5 m/year), with only 4% of high accretion (20.5 to 31.5 m/year). Dereli and Tercan, (2020), estimated the shoreline change of Salda Lake, Turkey, using DSAS tool and Modified Normalized Difference Water Index (MNDWI). They indicated that historical satellite images along with statistical parameters can be used to analyze shoreline change. Muskananfola et al., (2020), conducted a study to analyze shoreline change in Sayung Beach on the northern coast of Indonesia, for a period of 24 years (from 1994 to 2018), using Landsat 5, 7 and Sentinel-2. The statistical analysis of their study was done by DSAS tool. Considering literature reviews and the condition of our study area, we decided to employ Sentinel-2 satellite images, NDWI band ratio, and DSAS tool to calculate the seasonal river of Tiab Estuary's shoreline transformation.

## Study area

Tiab estuary is located 30 km south of Minab city and 7 km away from the coast of Strait of Hormuz, between latitudes 27.083693° to 27.116510° N and longitudes 56.816082° to 56.874818° E (Fig. 1) (Ghaderi and Rahbani, 2021). This estuary area is considered one of the most important estuaries in Iran which is covered with mangrove forest and is one of the few navigable estuaries in this country (Farahani et al., 2006; GHANBARI and MALEK, 2007). The main river of the estuary started from the northeast of Tiab village and enters the Persian Gulf with several branches (Fig. 1C). According to Mao et al., (2004) tidal activity is the main cause of disturbance and turbulence in estuary. The tide in the area is a mixed semidiurnal and is categorized as microtidal with a level of 1 to 2 m tidal range (Ershadi et al., 2013; Fayyaz et al., 2019; Ghaderi and Rahbani, 2021). This estuary has been recently faced numerous sedimentation problems, which has influenced the navigation in the inlet of the estuary and some branches significantly (Ghaderi and Rahbani, 2021). According to Ghaderi and Rahbani (2021) Tiab estuary is mainly influenced by tidal flood, as a result of which suspended sediments enter the estuary with the food tidal current and does not return to the sea due to the decrease in the ebb flow. According to them this issue is the main reason for the high volume of sedimentation in this estuary.

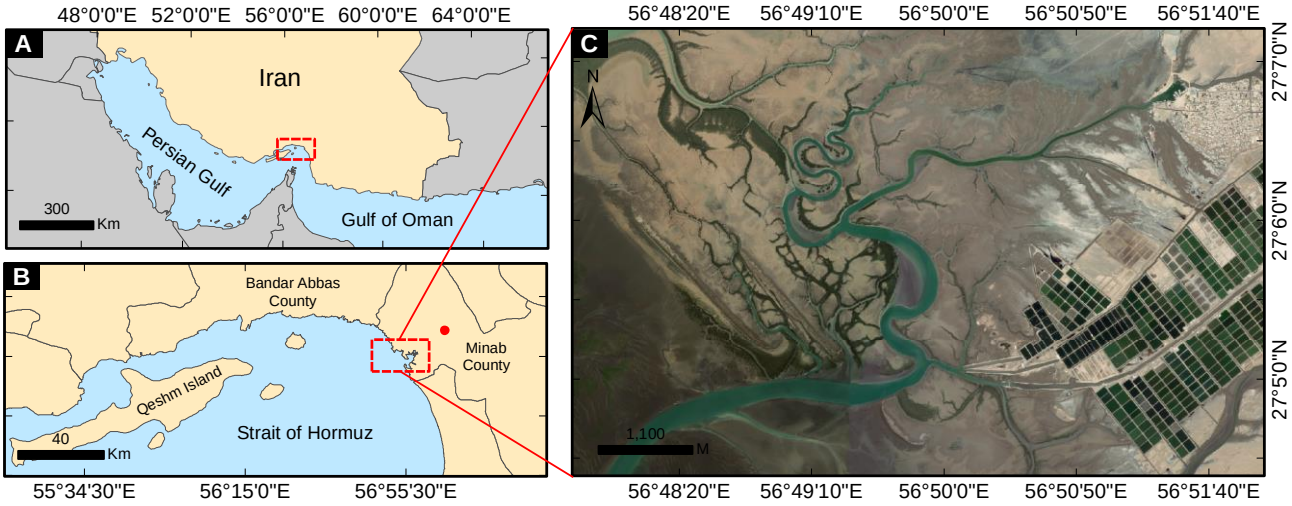


**Figure 1. The study area, A and B) location of the study area. C) Aerial image of Tiab estuary (The red dot is the meteorological station of Minab county)**

In addition to the tide, we suspected that the local wind conditions might influence the Tiab estuary. Even if estuary areas are mainly protected from waves and wave energy (Cowart et al., 2011), seasonal variation in wind pattern might be responsible for rare wave pattern in the area. The data from the synoptic station of Minab city (Iran Meteorological Organization) has been used to study the wind situation in the region (red point in Fig. 1 B). The statistical information of wind speed and direction for the years 2019 and 2020 is shown in Figure 2 for two seasons of summer and winter. According to the figure considerable deviation exists between the wind speed distribution of winter and summer. Such a deviation has been also stated in other studies (Kamranzad, 2018). The median wind speed of 2019 and 2020 is 1.0 and 1.6 m/s in winter and 2.0 and 2.7 m/s in summer, respectively. We therefore, decided to investigate the possible effect of this seasonal deviation for short-term transformation of the river's shoreline. We referred to Bolbasova et al., (2019) and Wu and Shi, (2022) statements that the median index provides a more accurate view of the speed difference. The kurtosis of the wind speed histogram curve is higher in the summer than in the winter, and the curve is slightly tilted towards the fourth quarter. In addition to the wind speed condition,

the wind direction is an important issue for wave generation and direction. Figure 2 shows that the wind direction in summer is mainly SSW, while during the winter, the distribution of wind direction is totally diverse. The histogram curve in the summer season is close to the standard normal distribution form, but in the winter season, it is quite wide and the wind direction is slightly closer to the north. The median wind direction of the years 2019 and 2020 are 140 and 118.9 degrees for the winter and 200 and 203.2 degrees for the summer respectively.

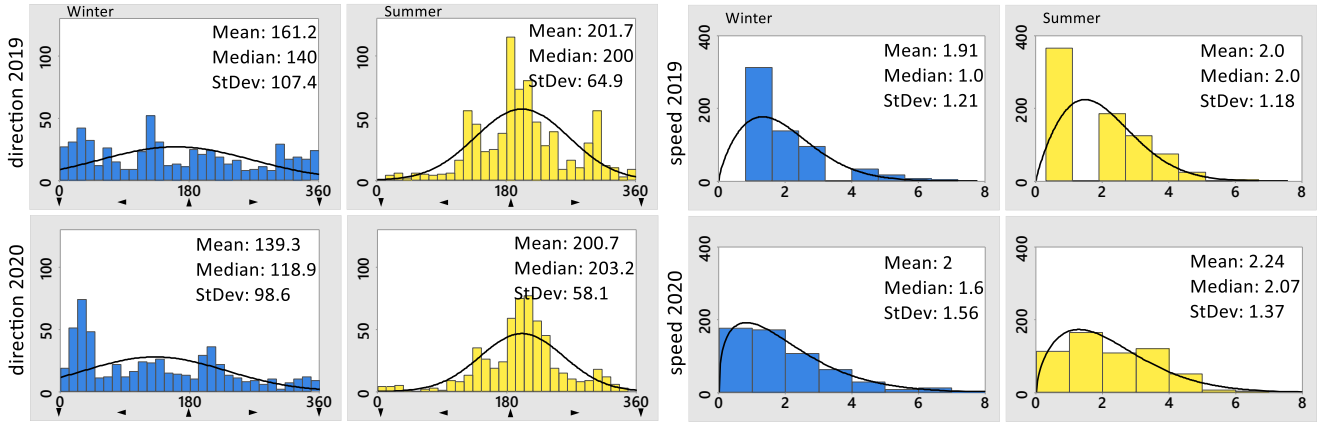


**Figure 2. Histogram of wind speed and direction during 2019 and 2020 in the Tiab region for summer (yellow), and winter (blue)**

## 2. Materials and methods

### Data collection

In order to investigate the short-term transformation of shoreline of the river, the RS technique has been used, employing Sentinel-2 satellite data with temporal resolution of once every five days, and spatial resolution of 10 m. Fine spatial resolution of 10 m of the Sentinel-2 satellite is a fair reason for scientists to employ them for studying small-scale phenomena and environments (such as the Tiab estuary) (Warnasuriya et al., 2020). It has been the object in so many studies among them Ghaderi and Rahbani, (2022, 2020b, 2020a); Mitri et al., (2020); Spinosa et al., (2021); and Drusch et al., (2012). The required satellite images are obtained from the Copernicus Open Access Hub of the ESA base (ESA, 2020). Taking into account restrictions for image selection due to the cloud coverage and dissimilarity in water level, we could derive out just four images of 2019/09/01, 2020/04/12, and 2019/13/06, 2020/02/06, for winter and summer seasons respectively. It should be emphasized that the Similarity in tidal water level is very important for studying shoreline transformation, especially for small-scale study areas (Boak and Turner, 2005; Ghaderi and Rahbani, 2020a). The water level in the selected images of Tiab estuary is between 0.5 and 0.6 m (Table 1). Besides, we selected those images when the amount of atmospheric precipitation was zero.

L1C satellite images of the Sentinel-2 are geometrically and radiometrically corrected (Barsi et al., 2018), but it is necessary to make atmospheric corrections to the images. Case 2 Regional Coast Color is an efficient algorithm for atmospheric correction of coastal-sea environments (Brockmann et al., 2016); therefore, this algorithm has been used in this study following previous literatures such as Ghaderi and Rahbani, (2020a), Pereira-Sandoval et al., (2019), and Ghaderi and Rahbani, (2022).

**Table 1. Information of satellite images used in the study**

| Date | Season | Satellite Imagery Products | Water Level (m) | Precipitation |
|---|---|---|---|---|
| 2019/09/01 | Winter | S2B_MSIL1C | 0.6 | 0 |
| 2019/13/06 | Summer | S2A_MSIL1C | 0.5 | 0 |
| 2020/04/12 | Winter | S2A_MSIL1C | 0.6 | 0 |
| 2020/02/06 | Summer | S2B_MSIL1C | 0.6 | 0 |

### Shoreline extraction

Considering the spectral behavior of satellite bands, the two features of water and land can be separated from each other, since each of them responds differently to different wavelengths. Body of water reflects low radiation and mainly absorbs visible to infrared wavelengths (Patel et al., 2021), but Land mainly reflects infrared wavelengths. Thus, by using two bands of Green and near-infrared in NDWI index (eq. 1), it is possible to produce the best distinction between water and land features (McFEETERS, 1996). The green ($B_{GREEN}$) and near-infrared bands ($B_{NIR}$) of the MSI sensor of the Sentinel-2 satellite are known as bands 3 and 8, respectively, and their average wavelength is 0.560 and 0.842 μm, respectively (Ghaderi and Rahbani, 2022; Patel et al., 2021).

$$NDWI = \frac{B_{GREEN} - B_{NIR}}{B_{GREEN} + B_{NIR}} \quad (1)$$

Applying the NDWI index results to the corrected images, a raster file (Fig. 3A) can be extracted, from which a bimodal distribution (Fig. 3B) of the area can be achieved. According to the raster file, the values of -1 represent the pixels with the feature of water, and the values of +1 represent the feature of land. In order to create a border between the body of water and the land (shoreline), it is sufficient to determine an optimal numerical value separating the two environments based on the histogram diagram. Supervised and unsupervised classification methods are available for separating these two features, in which we used two algorithms of the unsupervised classification method; K-means and Expectation-Maximization (EM) for this research. Unsupervised K-means classification has the ability to distinguish both features with optimal accuracy (Ahmed and Akter, 2017; Al-doski et al., 2013; Li and Wu, 2012). The basis of the k-means clustering algorithm is to minimize the cluster performance index according to the error square and the error criterion (eq. 2) (Li and Wu, 2012; Oliver et al., 2006).

$$e^2(K) = \sum_{k=1}^{K} \sum_{i \in C_k} (x_i - c_k)^2 \qquad (2)$$

where $c_k$ is the center of cluster $C_k$ and $K$ is the number of clusters (representative of prediction). The output result of the K-means algorithm is shown in Figure 3C. The result of the EM clustering algorithm is developed on the basis of artificial neural networks (Moser, 2002; Pôssa et al., 2018) (Figure 3D). One of the desirable features of the EM algorithm is its optimal performance in images with limited pixels (ESA, 2021; Ghaderi and Rahbani, 2022).

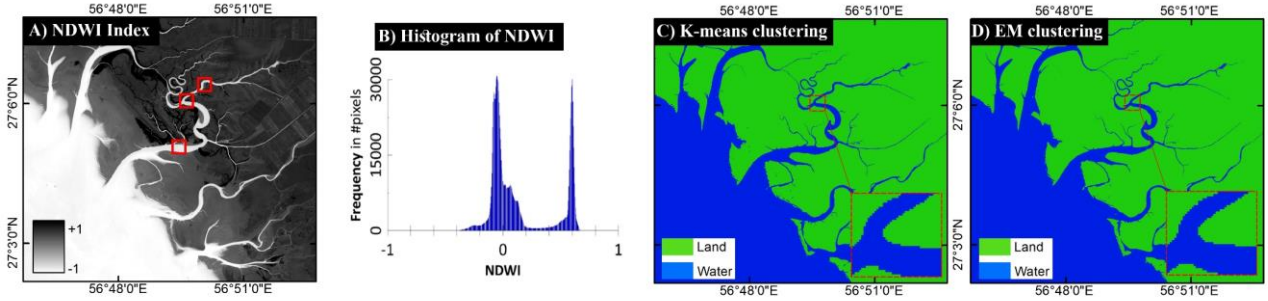


**Figure 3. A) Raster file of NDWI index, B) bimodal distribution of NDWI, C and D) K-means and EM clustering of NDWI raster file, respectively (red boxes in A are used to compare the accuracy of the two algorithms)**

**Detecting shoreline transformation**

The raster files of all four images resulting from the classification are converted into lines using ArcMap program, for statistical comparison of shorelines. The DSAS extension, developed by the United States Geological Survey, has the ability to assess the state of shoreline transformation using various statistical indicators (Thieler et al., 2009). The SCE index calculates the greatest distance between shorelines irrelevant to time, and always provides a positive number (Equation 3). This method for shoreline transformation detection has previously employed and confirmed by scientists such as Ghaderi and Rahbani, (2020b), (2020a); Muskananfola et al., (2020); Nassar et al., (2019); and Nath et al., (2022).

$$SCE = L_1 - L_2 \qquad (3)$$

where $L_1$ and $L_2$ are shorelines with the largest distance from each other. Since we employed and compared the shorelines of the two years, the obtained results only express the amount of transformation. (Himmelstoss et al., 2018; Thieler et al., 2009).

**Accuracy assessment**

The efficiency of unsupervised classification always depends on the accuracy level of each algorithm (Islam et al., 2021). Accuracy assessment of K-means and EM clustering algorithms has been done according to two statistical parameters Cohen's kappa coefficient (Rosenfield and Fitzpatrick-Lins, 1986) and confusion matrix. Overall accuracy is calculated using equation 5 (Congalton and Green, 2019), And Cohen's kappa coefficient is calculated using equation 6. For the sake of accuracy estimation the accuracy of the clustering algorithm is compared with User accuracy (Rosenfield and Fitzpatrick-Lins, 1986).

$$Overall\ accuracy = \frac{\sum_{i=1}^{r} n_{ii}}{n} \qquad (5)$$

$$K_c = n \sum_{i=0}^{r} n_{ii} - \sum_{i=0}^{r} \frac{n_{icol} n_{irow}}{n^2} - \sum_{i=0}^{r} n_{icol} n_{irow} \qquad (6)$$

$n_{ii}$ is the number of correctly classified pixels in each class; $n$ is the total number of pixels in the confusion matrix, $r$ is the number of rows, and $n_{icol}$ and $n_{irow}$ are the total column (reference data) and row (predicted

classes), respectively (Congalton and Green, 2019; Liu et al., 2007). To check the total accuracy, three boxes of 500 m × 500 m were considered in three areas of Tiab estuary (Figure 3A) . Comparing User accuracy with K-means and EM algorithms, Cohen's kappa coefficient and Overall accuracy were calculated. The results of the EM algorithm show that the kappa coefficient is 0.77 and the K-means algorithm is 0.94, and the overall accuracy is 88.7% and 96.8%, respectively. Therefore, K-means classification results were considered for clustering.

## 3. Result

### Seasonal shoreline transformation

Since we deal with the shoreline transformation of a river in an estuary in this research, hereafter we refer to the two sides of river as left side and right side facing toward the Persian Gulf. Figure 4 shows the transformation of the river shoreline between the two seasons of summer and winter with 10 m long transects. The river shoreline consists of 1500 transects, transects L-TID 1 to L-TID 718 correspond to the left side, and transects R-TID 1 to R-TID 728 correspond to the right side. The rate of seasonal shoreline transformation for the year 2019 (red graph) and 2020 (blue graph) are presented in this figure according to the SCE indexes. Based on SCE index the left side shore of the river averagely transformed 15.18 and 17.19 m during the years 2019 and 2020 respectively, with the standard deviation of 29.77 and 30.85 (minimum value for both is zero and The maximum is 206.15 and 221.99 m respectively). The results clearly indicates that seasonal shoreline transformation of the left side follows similar pattern during 2019 and 2020. The correlation coefficient (CC SCEL) of transformation in these two years is 0.90. The averaged shoreline transformations of the right side according to SCE index are 16.94 and 11.93 m in 2019 and 2020, respectively, and their standard deviations are 15.11 and 16.93 (the minimum for both is zero and the maximum is 134.85, and 138.54 m, respectively). The correlation coefficient (CC SCER) of shoreline transformation in these two years is 0.68. The results show that the averaged seasonal transformation of the left side is more than that of right side of the river. The overall correlation coefficient (CC SCE) for the shoreline transformation of the river in 2019 and 2020 is equal to 0.84.

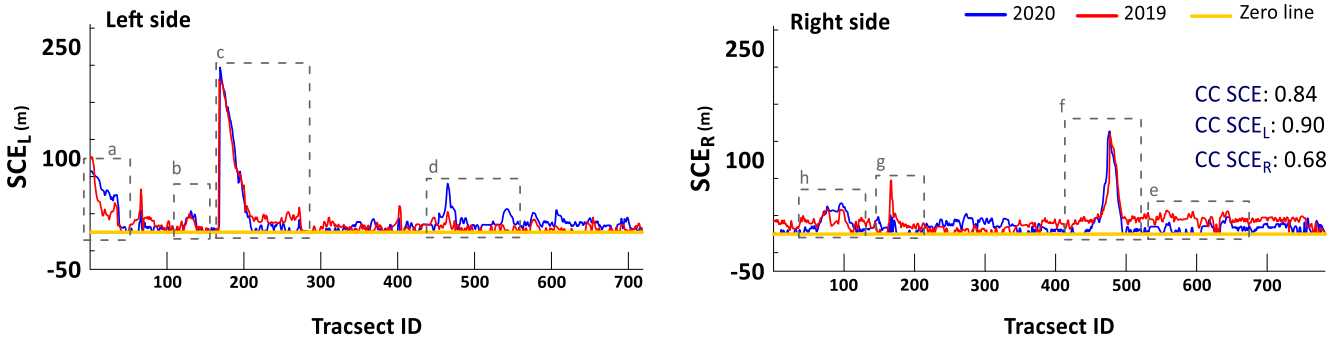


**Figure 4. Rate of seasonal shoreline transformation of Tiab estuary based on SCE and NSM indexes for the year 2019 (red) and 2020 (blue).**

### Shoreline transformation in upstream and downstream

We used SCE index to trace the shoreline transformation of the river in upstream (farther from the Persian Gulf) (Fig. 5) and downstream (entrance of the Persian Gulf) (Fig. 6) for the two years of 2019 and 2020. Calculations revealed that coveraged area of Tiab estuary in winter time is 112.43 and 116.78 hectares, and in summer time is 93.19 and 96.53 hectares for the years 2019 and 2020, respectively. These values indicate that the area of the estuary is more than 10 hectares smaller in summer time than in winter time. As an instant we refer to sections f19 and f20 of upstream river (Fig. 5) and sections a19, a20, c19, and c20 of downstream river (Fig. 6).

At the upstream of the river f19 and f20 of Fig. 5 shoreline transformation is significant between 45 to 200 m in both years of 2019 and 2020. This area faces high erosion and accretion due to the curves of the estuary. The only deviation between the two years of this study are the small area of d20 (Fig 5), where the transformation of about 45 to 60 m is detected only for the year 2020, and e19 (Fig 5), where the transformation of approximately 20 to 45 m is detected only for the year 2019. Since this area are located upstream of the river their transformation are more likely to be influenced by human activities in these areas and are to be more studied. Most part of the river faces transformation of less than 20 m. Shoreline transformation at the inlet of the estuary (a19 and a20 in Fig. 6) is between 45 and 120 m for both the years of 2019 and 2020 (erosion type). This is the area located at a curvature and also covered by mangrove forests, which slows down the hydrodynamic conditions thus cuses sedimentation which varies seasonally. At the left side, opposite side of the river, (h19 and h20 of Fig. 6) shoreline transformation is between 20 and 45 m (erosion type). This area is located on the other side of the curvature. Thus it is expected the variation of shoreline in this part influenced by the other side of the

river (a19 and a 20). This claim can be exactly applied to the areas b and g of Fig. 6, at second curvature of the downstream estuary. Area c in downstream river (Fig 6) faces the highest transformation for both 2019 and 2020, with the transformation between 45 and 200 m, which causes a large area of the estuary to be exposed in summer time. According to Ghaderi and Rahbani, (2021), current speed reduces significantly at this area and causes the accretion of suspended sediments, thus the concentration of Total Suspended Solids (TSS) in this curve is relatively high, which causes high deposition at the area.

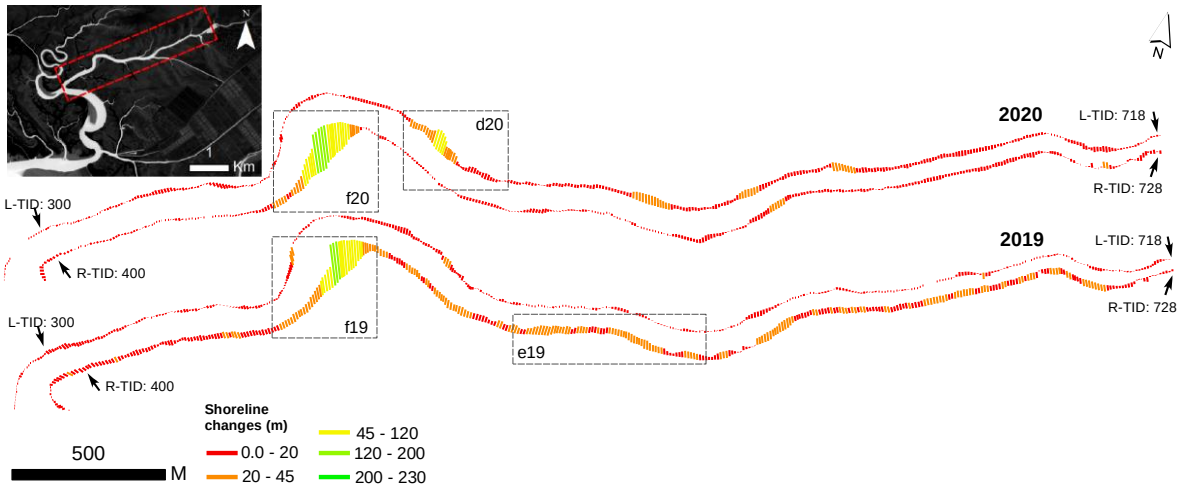


**Figure 5. Seasonal shoreline transformation of the downstream river at upstream of Tiab estuary based on the SCE index for the years of 2019 and 2020**

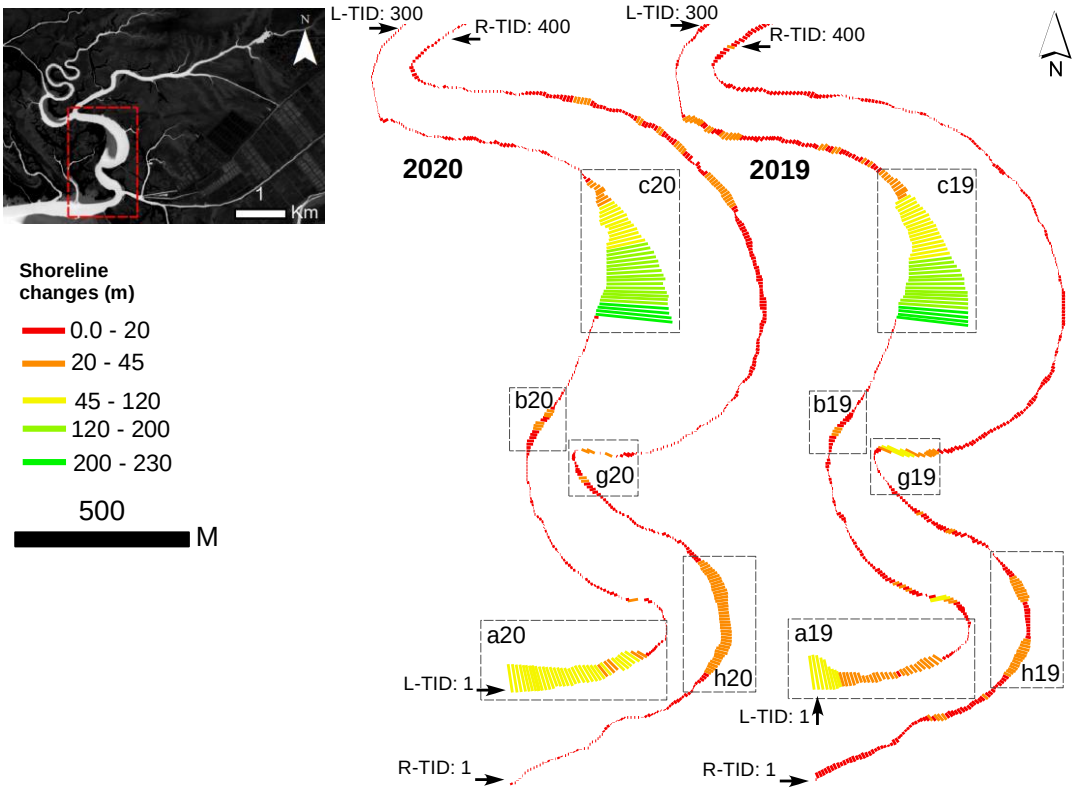


**Figure 6. Seasonal shoreline transformation of the downstream river at Tiab estuary based on the SCE index for the years 2019 and 2020**

## 4. Conclusions

The shoreline transformation of river in Tiab estuary shoreline, influenced by wind characteristics, is studied seasonally for the two years of 2019 and 2020. Considering the altering of the wind direction during summer and winter we focused on the shoreline transformation influenced by this factor. We detected similar behavior of shoreline transformation including erosion and accretion and the rate of transformation for both years. We also detected severe transformation in certain areas of the river especially downstream of the river, where the curvature exists in the channel and where the mangrove forests grow. However, the most part of the shoreline faces low transformation between

0 and 20 m. The upstream river faces the smallest transformation and some solely transformation is detected which was suspected to be due to the human activities. The highest rate of transformation in both up and downstream was detected at the curvature of the river, where the current slows down. It is expected that those part of the river with high rate of transformation, face significant changes in the long term. According to field visits, the first curvature in the downstream river (region h in this study) is eroded significantly, thus the width of the river will be increased in future. Also, in the second curvature in the downstream river (region c in this study), faces accretion in long term which makes the river relatively narrow, and this is reason for the restriction of navigation during most hours of a day which has been reported recently.

## 5. References


[1] Ahmed, K. R., & Akter, S. (2017). *Analysis of landcover change in southwest Bengal delta due to floods by NDVI, NDWI and K-means cluster with Landsat multi-spectral surface reflectance satellite data*. Remote Sensing Applications: Society and Environment, 8, 168–181.

[2] Al-doski, J., Mansor, S. B., Zulhaidi, H., & Shafri, M. (2013). *Image Classification in Remote Sensing* (Vol. 3, Issue 10, pp. 141–148).

[3] Barsi, J. A., Alhammoud, B., Czapla-Myers, J., Gascon, F., Haque, M. O., Kaewmanee, M., Leigh, L., & Markham, B. L. (2018). *Sentinel-2A MSI and Landsat-8 OLI radiometric cross comparison over desert sites*. In Eur. J. Remote Sens. (Vol. 51, Issue 1, pp. 822–837). https://doi.org/10.1080/22797254.2018.1507613

[4] Boak, E. H., & Turner, I. L. (2005). *Shoreline Definition and Detection: A Review*. Journal of Coastal Research, 214(4 (214)), 688–703. https://doi.org/10.2112/03-0071.1

[5] Bolbasova, L. A., Shikhovtsev, A. Y., Kopylov, E. A., Selin, A. A., Lukin, V. P., & Kovadlo, P. G. (2019). *Daytime optical turbulence and wind speed distributions at the Baikal Astrophysical Observatory*. Monthly Notices of the Royal Astronomical Society, 482(2), 2619–2626. https://doi.org/10.1093/mnras/sty2706

[6] Brockmann, C., Doerffer, R., Peters, M., Kerstin, S., Embacher, S., & Ruescas, A. (2016). *Evolution of the C2RCC neural network for Sentinel 2 and 3 for the retrieval of ocean colour products in normal and extreme optically complex waters*. ESASP, 740, 54.

[7] Congalton, R. G., & Green, K. (2019). *Assessing the Accuracy of Remotely Sensed Data*. CRC Press. https://doi.org/10.1201/9780429052729

[8] Cowart, L., Corbett, D. R., & Walsh, J. P. (2011). *Shoreline Change along Sheltered Coastlines: Insights from the Neuse River Estuary, NC, USA*. Remote Sensing, 3(7), 1516–1534. https://doi.org/10.3390/rs3071516

[9] Dereli, M. A., & Tercan, E. (2020). *Assessment of Shoreline Changes using Historical Satellite Images and Geospatial Analysis along the Lake Salda in Turkey*. Earth Sci. Inf., 13(3), 709–718. https://doi.org/10.1007/s12145-020-00460-x

[10] Drusch, M., Del Bello, U., Carlier, S., Colin, O., Fernandez, V., Gascon, F., Hoersch, B., Isola, C., Laberinti, P., Martimort, P., Meygret, A., Spoto, F., Sy, O., Marchese, F., & Bargellini, P. (2012). *Sentinel-2: ESA's Optical High-Resolution Mission for GMES Operational Services*. Remote Sensing of Environment, 120, 25–36. https://doi.org/10.1016/j.rse.2011.11.026

[11] Ershadi, S., Arasteh, M., & Tajziehchi, M. (2013). *Numerical Modeling of Flow Pattern Changes in Tidal Inlet of TIYAB Port*. Journal of Environmental and Earth Sciences, 11, 691–702.

[12] ESA. (2020). Copernicus Open Access Hub of the ESA. https://scihub.copernicus.eu/

[13] ESA. (2021). Expectation maximization (em) cluster analysis. ESA. https://www.brockmann-consult.de/beam/doc/help/clusteranalysis/EM.html

[14] Farahani, F., Farmohammadi, S. A., Golkhoo, S., & others. (2006). *Isolation of new isolate of micro algae Chlorella sp. Al-25 from Tiab estuary of Iran*.

[15] Fayyaz, M., Shafieefar, M., & Dastgheib, A. (2019). *Evaluation of the effects of sediment characteristics on long-term estuarine morphological modelling driven by waves and tides*. Applied Ocean Research, 92, 101919. https://doi.org/10.1016/j.apor.2019.101919

[16] French, P. (2002). *Coastal and estuarine management*. Routledge.

[17] Ghaderi, D., & Rahbani, M. (2020a). *Detecting shoreline change employing remote sensing images (Case study: Beris Port-east of Chabahar, Iran)*. Int. J. Coastal Offshore Eng., 3, 1–8. https://doi.org/10.29252/ijcoe.3.4.1

[18] Ghaderi, D., & Rahbani, M. (2020b). *Shoreline change analysis along the coast of Bandar Abbas city, Iran using remote sensing images*. Int. J. Coastal Offshore Eng., 4(2), 51–64. http://ijcoe.org/article-1-214-en.html

[19] Ghaderi, D., & Rahbani, M. (2021). *Tracing suspended matter in Tiab estuary applying ANN and Remote sensing*. Regional Studies in Marine Science, 44, 101788. https://doi.org/10.1016/j.rsma.2021.101788

[20] Ghaderi, D., & Rahbani, M. (2022). *Mud volcano as a feature of emergence in Caspian Sea*. Oceanologia. https://doi.org/10.1016/j.oceano.2022.03.006

[21] GHANBARI, F. M., & MALEK, M. (2007). *Permanent intertidal fish from the Persian Gulf and Gulf of Oman, Iran*.

[22] Himmelstoss, E. A., Henderson, R. E., Kratzmann, M. G., & Farris, A. S. (2018). *Digital shoreline analysis system (DSAS) version 5.0 user guide*. https://doi.org/https://doi.org/10.3133/ofr20181179

[23] Islam, M. S., Uddin, M. A., & Hossain, M. A. (2021). *Assessing the dynamics of land cover and shoreline changes of Nijhum Dwip (Island) of Bangladesh using remote sensing and GIS techniques*. Reg. Stud. Mar. Sci., 41, 101578. https://doi.org/10.1016/j.rsma.2020.101578

[24] Kamranzad, B. (2018). *Persian Gulf zone classification based on the wind and wave climate variability*. Ocean Engineering, 169, 604–635. https://doi.org/10.1016/j.oceaneng.2018.09.020

[25] Li, Y., & Wu, H. (2012). *A Clustering Method Based on K-Means Algorithm*. In Physics Procedia (Vol. 25, pp. 1104–1109). https://doi.org/10.1016/j.phpro.2012.03.206

[26] Liu, C., Frazier, P., & Kumar, L. (2007). *Comparative assessment of the measures of thematic classification accuracy*. Remote Sensing of Environment, 107(4), 606–616. https://doi.org/10.1016/j.rse.2006.10.010

[27] Mao, Q., Shi, P., Yin, K., Gan, J., & Qi, Y. (2004). *Tides and tidal currents in the Pearl River Estuary*. Continental Shelf Research, 24(16), 1797–1808. https://doi.org/10.1016/j.csr.2004.06.008

[28] McFEETERS, S. K. (1996). *The use of the Normalized Difference Water Index (NDWI) in the delineation of open water features*. Int. J. Remote Sens., 17(7), 1425–1432. https://doi.org/10.1080/01431169608948714

[29] Mitri, G., Nader, M., Abou Dagher, M., & Gebrael, K. (2020). *Investigating the performance of sentinel-2A and Landsat 8 imagery in mapping shoreline changes*. Journal of Coastal Conservation, 24(3), 1–9.

[30] Moser, G. (2002). *Unsupervised change-detection methods for remote-sensing images*. Opt. Eng., 41(12), 3288. https://doi.org/10.1117/1.1518995

[31] Muskananfola, M. R., Supriharyono, & Febrianto, S. (2020). *Spatio-temporal analysis of shoreline change along the coast of Sayung Demak, Indonesia using Digital Shoreline Analysis System*. Regional Studies in Marine Science, 34, 101060. https://doi.org/10.1016/j.rsma.2020.101060

[32] Nassar, K., Mahmod, W. E., Fath, H., Masria, A., Nadaoka, K., & Negm, A. (2019). *Shoreline change detection using DSAS technique: Case of North Sinai coast, Egypt. Mar*. Georesour. Geotechnol., 37(1), 81–95. https://doi.org/10.1080/1064119X.2018.1448912

[33] Nath, A., Koley, B., Saraswati, S., Choudhury, T., Um, J.-S., & Ray, B. C. (2022). *Geospatial analysis of short term shoreline change behavior between Subarnarekha and Rasulpur estuary, east coast of India using intelligent techniques (DSAS)*. GeoJournal. https://doi.org/10.1007/s10708-022-10683-8

[34] Oliver, A., Muñoz, X., Batlle, J., Pacheco, L., & Freixenet, J. (2006). *Improving clustering algorithms for image segmentation using contour and region information*. In 2006 IEEE International Conference on Automation, Quality and Testing, Robotics, AQTR (Vol. 2). https://doi.org/10.1109/AQTR.2006.254652

[35] Patel, K., Jain, R., Patel, A. N., & Kalubarme, M. H. (2021). *Shoreline change monitoring for coastal zone management using multi-temporal Landsat data in Mahi River estuary, Gujarat State*. Applied Geomatics, 13(3), 333–347. https://doi.org/10.1007/s12518-021-00353-8

[36] Pereira-Sandoval, M., Ruescas, A., Urrego, P., Ruiz-Verdú, A., Delegido, J., Tenjo, C., Soria-Perpinyà, X., Vicente, E., Soria, J., & Moreno, J. (2019). *Evaluation of Atmospheric Correction Algorithms over Spanish Inland Waters for Sentinel-2 Multi Spectral Imagery Data*. Remote Sens., 11(12), 1469. https://doi.org/10.3390/rs11121469

[37] Pôssa, É. M., Maillard, P., Gomes, M. F., Silva, I., & Leão, G. (2018). O*n water surface delineation in rivers using Landsat-8, Sentinel-1 and Sentinel-2 data*. In C. M. Neale & A. Maltese (Eds.), Proc. SPIE Oct. (Vol. 10783, p. 45). SPIE. https://doi.org/10.1117/12.2325725

[38] Rosenfield, G. H., & Fitzpatrick-Lins, K. (1986). *A coefficient of agreement as a measure of thematic classification accuracy. Photogramm. Eng*. Remote Sens., 52(2), 223–227.

[39] Schoellhamer, D. H. (2002). *Variability of suspended-sediment concentration at tidal to annual time scales in San Francisco Bay, USA*. Continental Shelf Research, 22(11–13), 1857–1866. https://doi.org/10.1016/S0278-4343(02)00042-0

[40] Spinosa, A., Ziemba, A., Saponieri, A., Damiani, L., & El Serafy, G. (2021). *Remote Sensing-Based Automatic Detection of Shoreline Position: A Case Study in Apulia Region*. J. Mar. Sci. Eng., 9(6), 575. https://doi.org/10.3390/jmse9060575

[41] Thieler, E. R., Himmelstoss, E. A., Zichichi, J. L., & Ergul, A. (2009). *The Digital Shoreline Analysis System (DSAS) version 4.0-an ArcGIS extension for calculating shoreline change*. https://doi.org/https://doi.org/10.3133/ofr20081278

[42] Warnasuriya, T. W. S., Kumara, M. P., Gunasekara, S. S., Gunaalan, K., & Jayathilaka, R. M. R. M. (2020). *An Improved Method to Detect Shoreline Changes in Small-Scale Beaches Using Google Earth Pro*. Marine Geodesy, 43(6), 541–572. https://doi.org/10.1080/01490419.2020.1822478

[43] Wu, J., & Shi, Y. (2022). *Changes in surface wind speed and its different grades over China during 1961–2020 based on a high-resolution dataset*. International Journal of Climatology, 42(7), 3954–3967. https://doi.org/10.1002/joc.7453